Pergamon

Journal of Structural Geology, Vol. 18, No. 5, pp. 595 to 614, 1996

0191-8141/96 $15.00 + 0.00

0191-8141(95)00124-7

Description and kinematics of the SE Loreto basin fault array, Baja California Sur, Mexico: a positive field test of oblique-rift models

PAUL J. UMHOEFER and K. A. STONE

Department of Geology, Northern Arizona University, Flagstaff, AZ 86011, U.S.A.

(*Received* 28 *November* 1994; *accepted in revised form* 22 *September* 1995)

Abstract—We present the results of mapping and kinematic analysis on an ~18 km2 array of normal and oblique-slip faults in the SE Loreto basin, near Loreto, Baja California Sur, Mexico. The fault array developed on the western margin of the Gulf of California in late Pliocene time, during the early part of the modern stage of oblique rifting of the gulf. The SE Loreto fault array is an antithetic transfer zone between two large, E-dipping normal faults. The fault array is coherent and formed in one episode. The dominant N- to NNE-striking faults primarily dip W and display nearly pure normal slip. More NE-striking faults show normal-sinistral slip and NW-striking faults have dextral-normal to dextral slip. N- to NW-striking faults have steeper dips and a greater component of dextral slip with more northwesterly strike. Bulk extension, based on strain analysis of faults with striae, is oriented nearly E–W with little plunge and consistent throughout the fault array.

The kinematic analysis of the SE Loreto fault array provides a well-constrained test of oblique-rift models. Our results support previous modeling of homogeneous extension in oblique-rifted margins when both instantaneous and finite strain are considered. Positive field tests of analytical and experimental models, such as this one, indicate that such models may be robust predictors of the obliquity of rifting in ancient mountain belts where brittle fault arrays are preserved, but plate motions are unknown. Copyright © 1996 Published by Elsevier Science Ltd

INTRODUCTION

Strain partitioning along obliquely convergent and divergent plate boundaries has been widely reported (e.g. Fitch 1972, Mount & Suppe 1987, Stock & Hodges 1989, Jackson 1992). These boundaries have zones of deformation hundreds of kilometers wide characterized by one or more major strike-slip or transform faults and a wide zone of contractional or extensional deformation dominated in the upper crust by either thrust or normal faults. Experiments and numerical models of oblique-divergent (or transtensional) plate boundaries predict specific strain patterns for a given amount of relative plate obliquity (McCoss 1986, Withjack & Jamison 1986, Tron & Brun 1991, Smith & Durney 1992, Teyssier *et al.* 1995). These models, however, are largely unconstrained by field studies that include detailed mapping and kinematic analysis of fault arrays along oblique-divergent margins where the boundary conditions are known. Field studies can test the nature of regional strain partitioning and the extent to which local strain patterns and kinematics are controlled by plate boundary conditions.

Here we report the results of detailed mapping and kinematic analysis of a relatively small fault array within the Pliocene–Quaternary Loreto basin in Baja California Sur, Mexico (Figs. 1 and 2). The Loreto basin lies along the Gulf of California, which contains a highly oblique-divergent plate boundary between the Pacific and North American plates (e.g. Larson *et al.* 1968, Angelier *et al.* 1981, Henry 1989, Lonsdale 1989, Stock & Hodges 1989, Zanchi 1994). Dextral transtensional

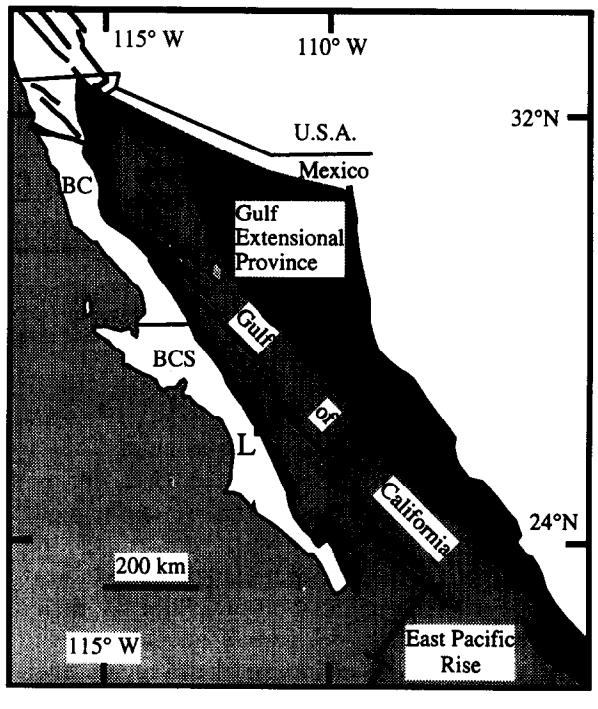

Fig. 1. Loreto basin (box near large 'L') and the major tectonic features of the Gulf of California region. BC = Baja California, BCS = Baja California Sur. The Main Gulf Escarpment is the wide line along the eastern coast of the Baja peninsula that defines the western edge of the Gulf Extensional Province.

deformation occurred within the basin during late Pliocene and Quaternary(?) time with the direction of bulk extension approximately E–W (Zanchi 1994). All of the faults in the SE Loreto fault array cut 2.6 to approximately 2.4 Ma marine and non-marine strata in the

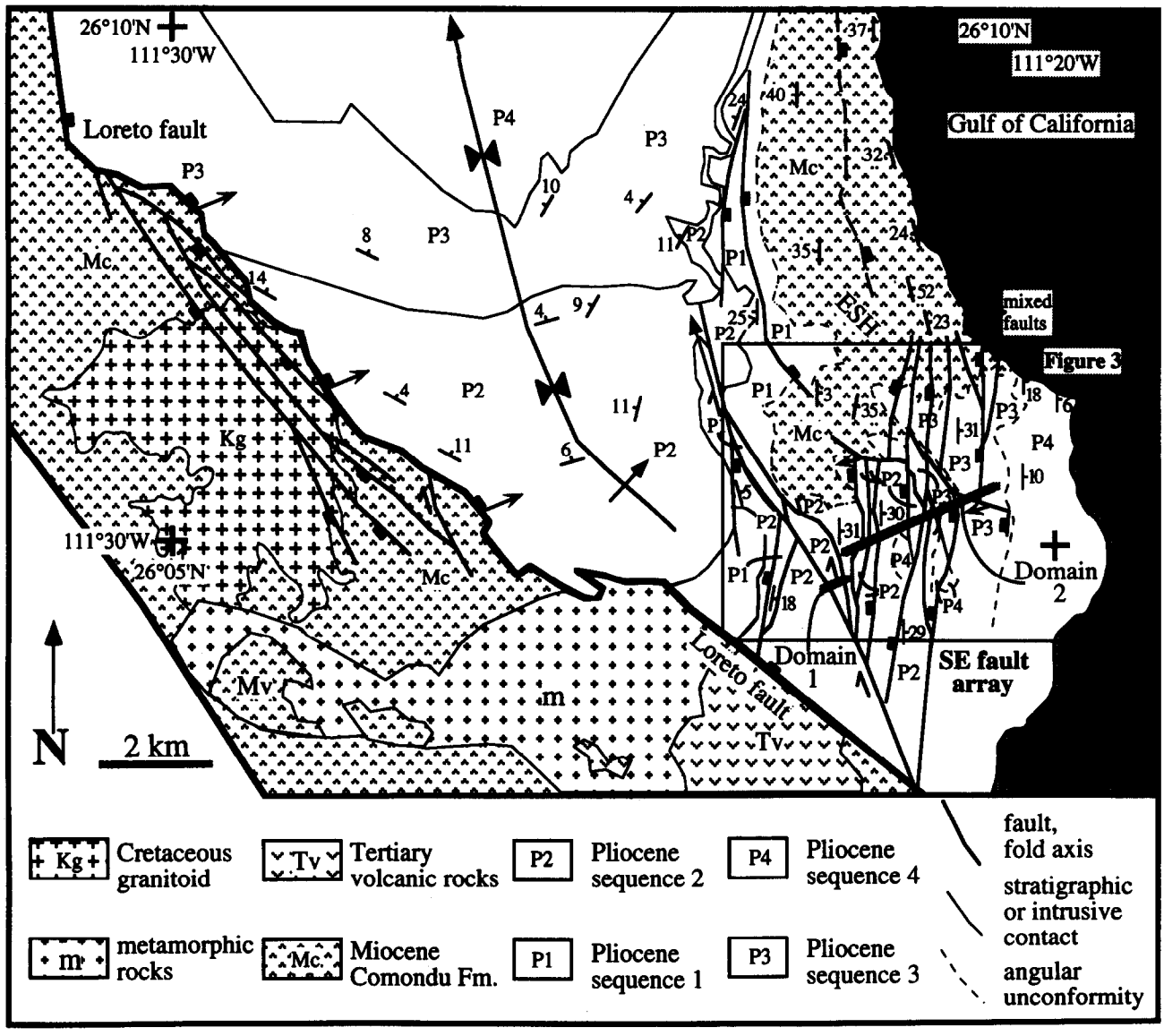

Fig. 2. Geologic map of southern Loreto basin (Pliocene strata) and surrounding area. Quaternary units are not shown. ESH is the eastern structural high of Umhoefer *et al.* (1994a) or the Cerro Microondas of Zanchi (1994). The city of Loreto is ~2 km south of the map on the coast. The area south of the Loreto fault is in part after McLean (1988).

southeast Loreto basin (Umhoefer *et al.* 1994a), and ~2.0 Ma strata are cut by only minor faults. Therefore faulting occurred mainly from ~2.4–2.0 Ma, during the modern phase of very oblique rifting in the Gulf of California region (Lonsdale 1989).

If our analysis of the SE Loreto fault array is indicative of regional strain along the Gulf of California, then it is relevant for testing model results on oblique rifting. Despite the relatively small size of the region encompassing the fault array (~18 km^2), we believe the fault array is representative of regional strain because: (1) it is well exposed and mapped in detail and kinematics are well described; (2) it is geometrically and kinematically coherent and therefore probably developed in a simple manner; (3) the overall extension direction from our study is similar within a few degrees to that from similar studies of Pliocene strata in the region (Angelier *et al.* 1981, Zanchi 1994); and (4) the SE fault array is part of a much larger fault system because it is an antithetic transfer zone between the southern Loreto fault and a coastal fault to the north. These points are discussed in more detail in later sections.

Importantly, our study is the first along the western margin of the Gulf of California in Baja California Sur that combines kinematic analysis of faults that cut Pliocene strata with detailed mapping (10:000 and locally 1:5000 scale) of the fault array, a scale of mapping that is necessary to understand the complex fault patterns. When these results from the SE Loreto fault array are compared to plate motions, it confirms essential elements of recent modeling of oblique-rift plate margins and offers insights into how transtensional plate margins behave.

GEOLOGIC SETTING

The Loreto basin is part of the Gulf Extensional Province (Umhoefer *et al.* 1994a, Zanchi 1994), a region of normal and strike-slip faults and basins that surrounds

the Gulf of California (Fig. 1) (Gastil *et al.* 1975, Stock & Hodges 1989). The western edge of the Gulf Extensional Province is the Main Gulf Escarpment, a major topographic break that is generally fault controlled and runs the length of the Baja California peninsula on its eastern side (Fig. 1). The Gulf Extensional Province is a relatively narrow onshore belt and marine shelf that contains syn-transform faults and isolated basins and lies between the Main Gulf Escarpment and the shelf-slope break in the Gulf of California. Most of the structures in the Gulf Extensional Province formed during the development of the Gulf of California over the past ~12 Ma (e.g. Gastil *et al.* 1975, Lonsdale 1989, Stock & Hodges 1989).

The Gulf Extensional Province is interpreted to have had two major stages of deformation with a transitional deformation stage between. A proto-gulf stage from ~12 to ~5 Ma was characterized by regional strain partitioning with ENE–WSW extension on NNW-striking normal faults in the Gulf of California region and major dextral-slip faulting on the Tosco–Abreojos fault system west of the Baja peninsula (e.g. Karig & Jensky 1972, Spencer & Normark 1979, Hausback 1984, Stock & Hodges 1989). Some interpretations of the southern San Andreas fault system in California suggest that some strike-slip faulting occurred in the Gulf of California during the proto-Gulf stage (e.g. Humphreys & Weldon 1991, Lyle & Ness 1991). A transitional stage may have existed from ~5 to 3.5 Ma when poorly organized strike-slip faulting in the Gulf of California was occurring at the same time as diminished strike-slip faulting on the Tosco–Abreojos fault west of Baja (Lonsdale 1989), which resulted in the Baja peninsula being a separate microplate during this stage. During the modern stage from ~3.5 Ma to the present, the transform-rift system formed that is currently in the deep marine of the Gulf of California (Lonsdale 1989). This stage was the first time in which essentially all of the plate boundary was localized along the transform-rift system in the Gulf of California (Lonsdale 1989).

Structures of the proto-gulf stage in the Loreto area are NW- and SE-striking normal faults that cut the Miocene Comondu Formation, but do not cut the Pliocene Loreto basin (Zanchi 1994). The Loreto basin formed within the modern stage of the evolution of the Gulf of California (Umhoefer *et al.* 1994a, Zanchi 1994), from ~3.5 Ma to the present. The main structures in the southern Loreto basin are the Loreto fault along the southwest margin of the basin, the eastern structural high along the present coast to the east, and the SE Loreto fault array of this study (Fig. 2) (Umhoefer *et al.* 1994a). The eastern structural high is a hangingwall high relative to the Loreto fault and is in the footwall of a fault zone that lies along its east (coastal) side. The high was active during sedimentation. Between the Loreto fault and the eastern structural high is a WSW-thickening wedge of strata that comprises most of the south-central basin; this area is a gently NNW-plunging, open syncline that formed as a broad hangingwall syncline along the Loreto fault (Fig. 2). The strata of the marine part of the basin are ~2.6 to ~2.0 Ma based on $^{40}Ar/^{39}Ar$ dating of four tuffs intercalated in the lower and upper parts of the section (Umhoefer *et al* 1994a). An undated non-marine section is immediately below the 2.61 Ma tuff and estimated to be ~3.5 to ~2.6 Ma.

The age and position of the SE Loreto fault array suggests that it was active mainly during late Pliocene time (Fig. 2). Many of the faults of the SE fault array cut strata of sequence 3; the lower part of sequence 4 is tilted by faulting while the upper part of sequence 4 has little tilt and is cut by small-displacement faults. By correlation to the south-central basin where the strata are well dated (Umhoefer *et al.* 1994a), sequence 3 in the SE basin is ~2.4–2.37 Ma and sequence 4 is ~2.0 Ma with a locally angular unconformity between them. Large parts of the fault array are directly linked and probably acted together. Therefore, we conclude that faulting occurred between ~2.4 and ~2.0 Ma, but it may have started earlier in the west because those faults cut only sequences 1 and 2.

The SE fault array is a transfer zone between the southeastern end of the Loreto fault to the south and the coastal fault zone to the north, both E-dipping structures (Fig. 2). We interpret the W-dipping SE fault array to be an antithetic transfer zone between these two large faults (Umhoefer unpublished data). The faults of the SE fault array probably extend to and merge with the Loreto fault, but the area where they merge is not well exposed. The SE fault array joins the coastal fault zone across an ~1 km wide complex accommodation zone (Fig. 2). The antithetic nature of the SE fault array relative to the Loreto fault zone (Fig. 2) is a common style of faulting in the hangingwall of a major normal fault (Withjack *et al.* 1995). The density of faults in the SE fault array makes the array anomalous in the Loreto basin (Fig. 2); we believe this localized high density of faults is the natural consequence of distributed faulting in the uppermost crust during regional extension.

DESCRIPTION OF SE LORETO FAULT ARRAY

Overview

The SE Loreto fault array is a dense network of anastomosing, domino-style normal, normal-oblique and dextral-normal faults. From map relations and kinematic data, the entire fault array is considered geometrically and kinematically coherent (as defined by Walsh & Watterson 1991). The array can be divided into two domain based on bedding and fault orientations (Figs. 3 and 4). Domain 1 is located along the western margin of the fault array and is bounded to the east and west by dominantly dextral, strike-slip to oblique-slip faults that strike approximately northwest and form a 300-m-wide anastomosing fault zone. Secondary faults strike north and merge into the dominant NW-striking faults. Bedding is dominantly E-dipping in domain 1 (Fig. 4), but varies considerably because of a few map-scale folds within the domain (Fig. 3). Faults of domain 1 die out

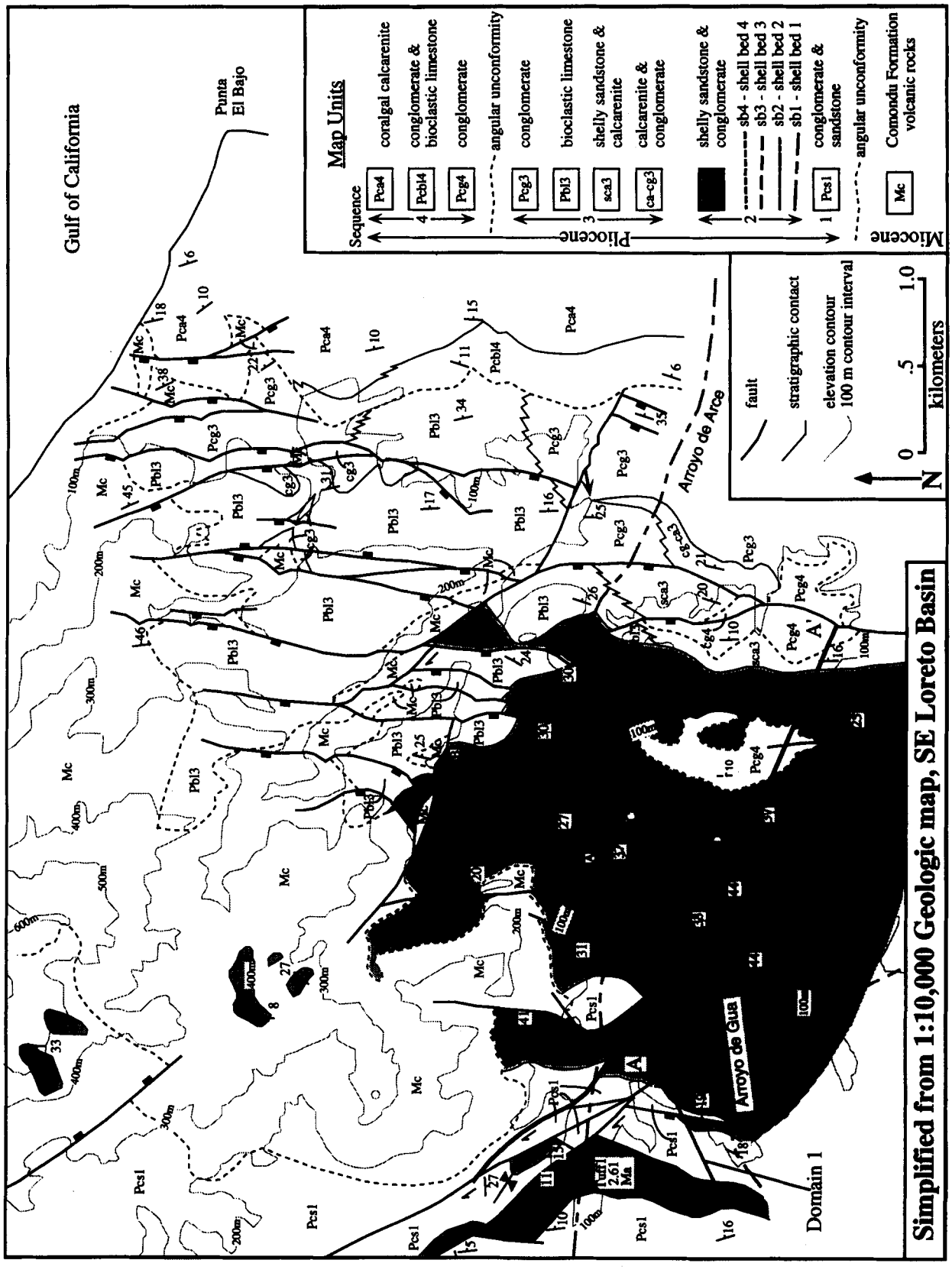

Fig. 3. Geologic map of the SE Loreto fault array. The map is simplified, but shows all of the major (tens of meters of offset) faults and marker shell beds. Domain 1 is indicated by the arrow in the lower left and bounded on the east by the thick-lined fault. Domain 2 is the remaining part of the fault array. The local strain accommodation zones are labeled A, B, C, D in boxes. Numerous small Quaternary terraces north of Arroyo de Gua and a large terrace south of Arroyo de Gua are not shown. Cross section A–A′ is shown as the thick line across the southern part of the map. The Corrugation fault is the oblique-slip fault ~0.5 km north of the eastern part of Arroyo de Arce.

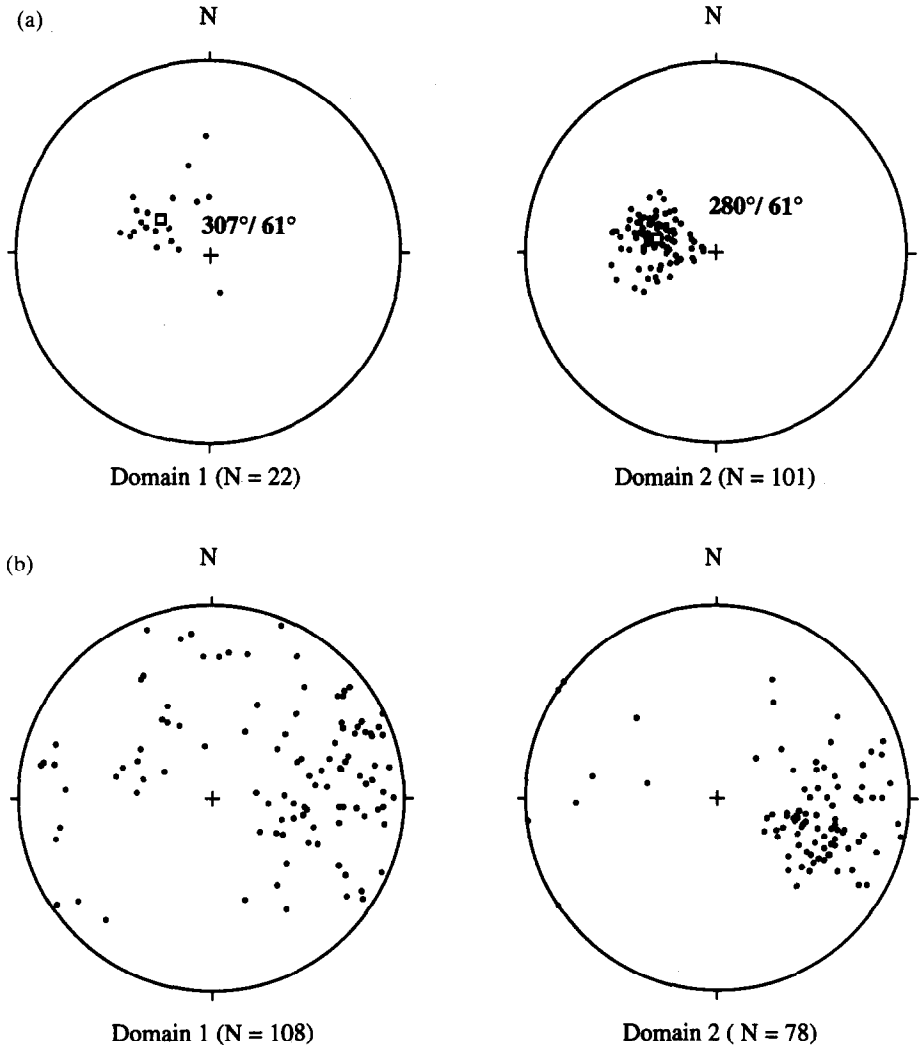

Fig. 4. (a) Equal-area stereograms of poles to bedding for the two domains. Dots represent poles; white-filled square is the vector mean for each population with the corresponding plunge and trend labeled. (b) Equal-area stereograms of poles to fault planes (dots) for the two domains.

into folds ~2 km north-northwest of the main map area in Figure 3 (Fig. 2). Domain 2 comprises the bulk of the SE Loreto fault array and consists of dominantly W-dipping, domino-style normal and oblique-slip faults, most of which splay and merge in an anastomosing fashion (Fig. 3). Bedding dips E at low to moderate angles (Fig. 4). Bedding in the eastern part of the domain, above an angular unconformity, dips 5–18° E, and decreases eastward across numerous intra-formational unconformities. Two prominent faults in domain 2 are WNW- to NW-striking transfer faults, including the well-exposed Corrugation fault described below (Fig. 3). Some of the faults in the western part of domain 2 merge into the main domain 1 faults. The other faults in domain 2 probably also join domain 1 faults farther south, but strata and faults are poorly exposed where many of these faults would join (Fig. 2). Many faults in domain 2 extend north into the Comondu Formation (Fig. 3), where they are difficult to detect. These faults probably connect to the coastal fault zone to the north (Fig. 2).

Fault separations were determined primarily from the offset of marker beds within marine strata and range from tens of cm to 200 m on individual faults. Fault slip was determined by using the separation information together with fault dip and the slip direction based on fault lineations. The blocks between faults of ~5–200 m offset are generally unfaulted and bedding orientation is consistent. Sub-meter scale faults are common in a few small domains near the junction of larger faults and these are interpreted as local zones of strain accommodation. The rotation of beds or blocks about vertical axes might be expected where dextral and normal faulting has occurred. Vertical-axis rotation of the entire SE fault array is difficult to evaluate. In local areas in domain 1 some rotation might have occurred because bedding is not systematically tilted toward the faults and folds are present. In contrast, over most of domain 1 and all of domain 2, bedding is systematically tilted toward the adjacent normal fault and strikes approximately parallel to the fault, a configuration that strongly suggests no local rotation about vertical axes. This conclusion may be violated in small blocks within the strain accommodation zones discussed below.

Description of faults

The fault breccia zones commonly grade from zones of intense cataclasis in the interior to widely spaced joints or small fractures on the exterior (Fig. 5a). Widths of fault breccia zones range from a few centimeters to well over 1 m (most are <50 cm), and some are relatively uniform within the same fault zone. Many faults within the study area display well-developed, but discontinuous, gouge zones that exhibit a great variation in thickness, from less than one centimeter to ten centimeters. A majority of the thicker gouge zones (>6 cm) are typically cut by small sub-fractures and thin slivers of host rock. Fault gouge is common in most faults with ~5 m or more offset (Figs. 5a–c). Most gouge in the study area is dominantly calcite and minor components of a clay-like mineral (palygorskite) and secondary carbonate (ankerite). A minor amount of fault gouge in the SE Loreto fault array is red clay in mm-scale layers that was derived from cataclasis of the host rock.

Although carbonate fault gouge may be initially formed by chemical precipitation of calcite and thus independent of cataclasis, once the material is deposited within the fault zone it is subject to deformation and shear strain. Typically, those faults with well-developed carbonate gouge zones exhibit a planar, schistose-like fabric oriented at 0 to ±45° to the shear plane (i.e. breccia and/or host rock boundary). Less common are planar anisotropies resulting from localized high shear strain sub-parallel to the shear zone boundary. Together, these structures form a composite (Fig. 5b) that is geometrically similar to *S–C* tectonites in ductile shear zones (Lister & Snoke 1984, Chester & Logan 1987).

The use of *S–C* fabric in fault gouge as a sense of separation indicator has been reported by several workers (e.g. Rutter *et al.* 1986, Chester & Logan 1987). *S*-foliation in gouge zones can form between 0° and ±45° to the shear plane, particularly in meter-scale and larger faults (Chester & Logan 1987, Evans 1988). Observed values for the study area range from +20° to +40°. Where the *S*-foliation plane–shear plane angle was measured, it provided a consistent normal down-to-the-west sense of separation, and in all places was consistent with stratigraphic evidence for separation.

'*S–C*' structures yield semi-quantitative kinematic information on sense of slip in oblique-slip faults, because the orientation of the *S*-foliation plane is a function of fault-slip obliquity. If a fault were purely dip-slip, an ideally formed *S*-foliation plane should possess the same strike as the fault plane and the intersection lineation between the *S*-foliation plane and fault plane would be horizontal and parallel to the strike direction. For example, fault lineations on a purely dip-slip fault should lie at 90° to the strike direction and hence to the fault plane–*S*-foliation intersection lineation. The striae and the fault plane–*S*-foliation intersection lineations were measured together on three faults to determine if this relation holds on oblique-slip faults. The angle between the two types of lineations on three faults is 68°, 61°, 70° (Fig. 6). These data suggest that there is a geometric–kinematic relationship between carbonate-gouge *S–C* composite structures and the direction of slip, but that it is not strictly orthogonal. Obviously the amount of data available for this comparison is small, and at best lends itself to a qualitative interpretation.

Abrasion striae and grooves are the most common lineation observed on fault surfaces (Fig. 5c). They are found on carbonate and red-clay fault-gouge surfaces, where they form short discontinuous segments with striae typically ranging between 5 and 8 cm long and approximately 1 mm wide. Grooves tend to be slightly wider, 2–5 mm, with small troughs 1–2 mm deep (Fig. 5c). Some larger and better exposed faults (e.g. the Corrugation fault) exhibit grooves and striae tens of centimeters long, but on average these lineations rarely exceed 10–15 cm in length. It is rare to find striae in host rocks, which may be due to the only moderate induration of the Pliocene rocks found in the study area; striae are most common in the fault gouge. Of the fault segments mapped with >10 m offset, 30–40% displayed reliable striae. Centimeter- to decimeter-scale faults commonly contain striae. Other less common fault lineations include tool tracks and minor corrugations, which usually lie sub-parallel to the fault striae. Tool tracks from discontinuous score marks 5–10 cm long and several millimeters deep. Grooves and tool tracks may be the same feature.

Some faults exhibit secondary fractures in both the footwall and hangingwall that subtend acute angles of ~35° or less with the fault plane (Fig. 5a). These fractures commonly extend 20–100 cm from the fault plane and rarely form conjugate pairs. These have been interpreted as R_1 Riedel shear fractures (Hancock 1985). Where these structures are well developed and the sense of offset clearly indicated, they consistently support other criteria for the sense of separation on the fault; however, such data were uncommon and thus Riedel fractures were seldom used for kinematic analysis.

Corrugation fault

There are two faults in domain 2 that strike at high angles to the dominant S-striking normal faults (Fig. 3). We interpret these two faults as transfer faults or cross faults that are an integral part of the fault array. They both terminate against large S-striking normal faults. Both faults have abundant kinematic indicators that indicate movement of the upper (southern) plate toward the WSW (~245–250°) (Fig. 7). This direction of movement is more southerly than the average trend of extension based on our kinematic analysis of the entire fault array. The difference in extension direction is taken up by a local zone of complex faulting adjacent to the western fault (Fig. 8b).

One of the transfer faults in domain 2, which we call the Corrugation fault, is located in the east-central part of the study area (Figs. 3 and 5d). This fault is of particularly interest because it confirms the use of abrasion striae as reliable kinematic indicators. The fault

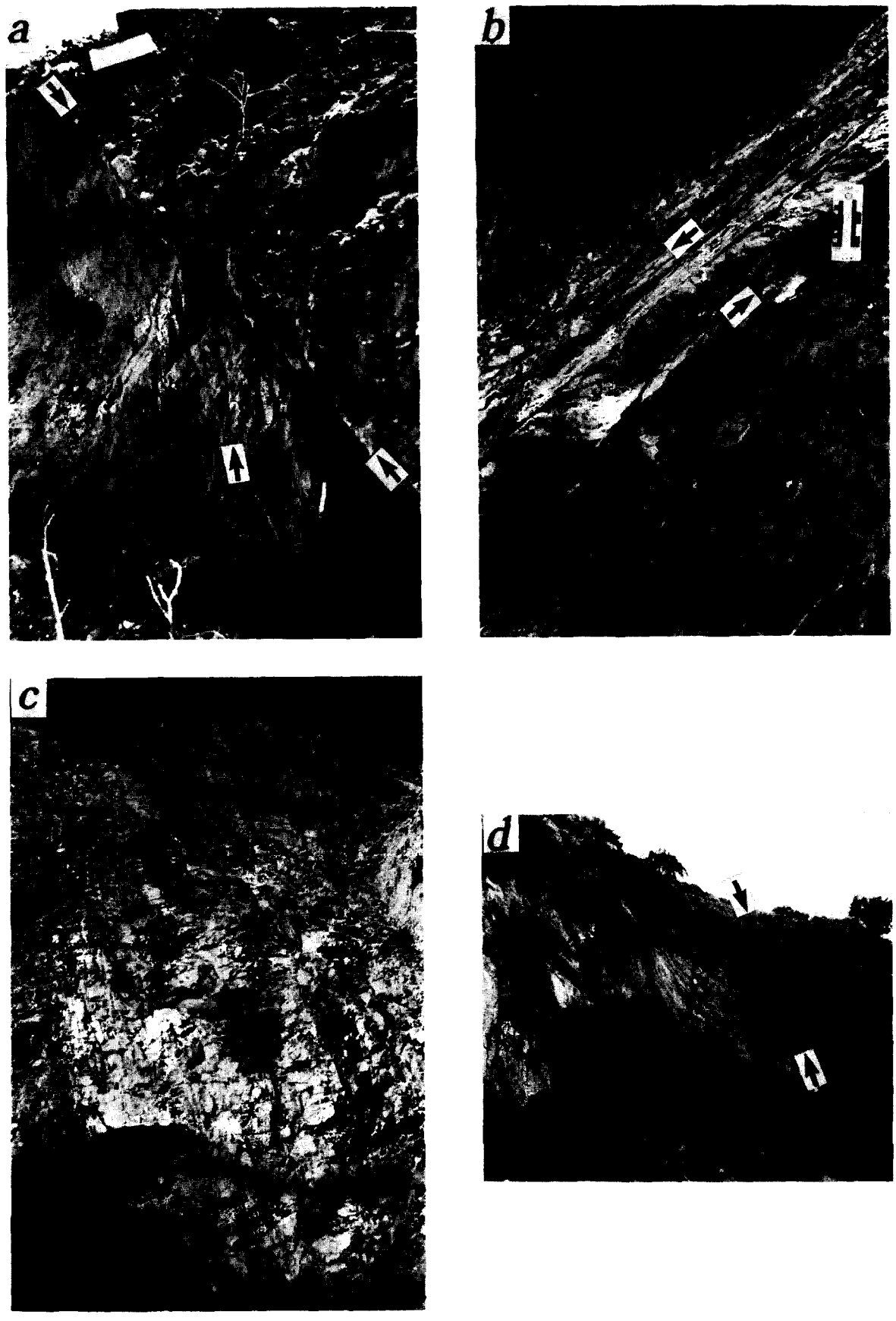

Fig. 5. (a) View to approximately 180° showing pervasive secondary fractures (lower arrow) in the footwall of a typical down-to-the-west (right in photo) normal fault. Fault marked by opposing arrows. Fractures have been interpreted as Riedel R_1 fractures (subvertical arrow). Map board in upper left is 30 cm across. (b) Cross-sectional view to the north of a carbonate gouge zone which has a well-developed *S*-foliation and *C*-shear plane. Arrows indicate movement direction and are parallel to the *C*-shear plane. The carbonate gouge zone is 5–7 cm thick. The fault is sinistral-oblique with 33 m of down-to-the-west separation (left in photo). (c) View of face of the footwall of a normal fault with grooves and striae well preserved in fault gouge (hammer handle points down dip). (d) View to the east showing the exposed section of the footwall of the Corrugation fault. Opposing arrows indicate the fault where both hangingwall conglomerate (to the right) and footwall carbonate (to the left) meet. The person is standing in the middle of a mega-corrugation.

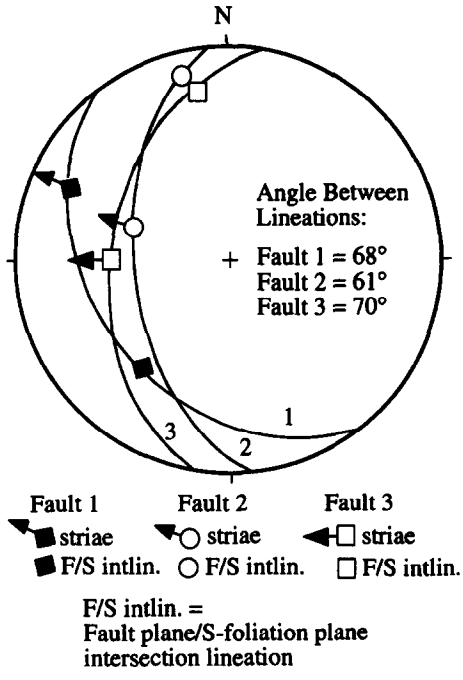

Fig. 6. Equal-area lower-hemisphere plots of three oblique-slip faults containing striae and well-developed *S*-foliation planes. Striae are compared to the orientation of the fault plane–*S*-foliation plane intersection lineation. Note that the angle between the two lineations is not the ideal 90°, but it is consistently a high angle. See text for discussion.

surface is extremely well exposed in one location, where it contains a variety of common and uncommon brittle fault-zone structures: abrasion striae, grooves or tool tracks, Riedel fractures, comb-style fractures, and minor, major, and two mega-corrugations (terminology after Hancock & Barka 1987). The most impressive features on the fault surface are the large-scale mullions (Fig. 5d). Hancock & Barka (1987) recognized similar features in the Yavansu fault zone in western Turkey and named these lineations 'corrugations', which are characterized by a crudely sinusoidal profile normal to their long axis. Three size classes of corrugations were noted on the Corrugation fault: minor (wavelengths 65–170 mm), major (240–450 mm) and mega (5000–16,000 mm) (corrugation size classification after Hancock & Barka 1987). Mega-corrugations of the same scale and shape as these are at ~100–250 m depth on an active normal fault of the West Mercer fault, South Oquirrh Mountain fault zone, Utah (Wu & Bruhn 1994).

The most important aspect of the Corrugation fault for kinematic analysis is the colinearity of the uncommon lineations (minor, major, mega-corrugations and tool tracks) and the common abrasion striae and grooves (Fig. 7). All lineations observed on the Corrugation fault are sub-parallel within ≤20° (Fig. 7) and yield a sense of slip down to the WSW, or dextral-normal, and the mean vector orientation of the crest axis is 43–247° (Fig. 7d). The vector mean of the minor and major corrugations, striae, grooves and tool tracks, is 49–243°, and when compared to the mega-corrugation axes are colinear to within <10° (Fig. 7e). This observation of colinear features confirms the validity of using striae and small grooves as indicators of the direction of fault slip where they are the only features present, as is common in other faults of the array.

Strain accommodation zones

Most of the fault blocks in the study area are structurally competent and exhibit little internal deformation. There are some areas between faults, however, which display centimeter- to meter-scale faulting and common antithetic and conjugate faults (Figs. 3 and 8). We call these areas strain accommodation zones, because we interpret them to be zones that accommodate small differences in strain between large-scale faults.

Four strain accommodation zones were studied (Fig. 8). Each of the zones lies between two or more fault strands with offsets >20 m that merge to form a wedge (Fig. 8a, c & d) or are adjacent to the join between an E-striking transfer fault and an S-striking normal fault (Fig. 8b). A commonality among the former three of the strain accommodation zones (Fig. 8a, c & d) is the presence of steeply-dipping antithetic (E-dipping) faults and/or conjugate fault pairs. Antithetic faults are not found in any of the major fault blocks in domain 2 and seem to only occur within these zones (compare Figs. 10 and 11). Two of these zones have areas of dense small-scale faults (Figs. 8b & c). In both cases, the small-scale faults are found where two large-scale faults merge. The lack of kinematic information from both large-scale faults precludes a definitive interpretation of why these zones formed. We suggest that the areas of small-scale faults accommodated some of the strain differences between the two large-scale faults. Finally, we note that two of these zones (Figs. 8a & d) have some of the only bedding with orientations that differ much from the mean orientation of bedding in domain 2, which suggests local rotations occurred around plunging axes.

One strain accommodation zone (Fig. 8c) has the only fault on which we observed two sets of striae with very different rake in close proximity, one strike slip and one oblique slip. However, they were not superposed and therefore relative timing not determined. A strike-slip fault and normal fault join near this location and therefore we interpret that this is a local feature. Significantly, this was the only fault in the whole fault array that had two striae with significantly different orientation. All other occurrences of two striae in close proximity were similar within about 5° (Fig. 8).

KINEMATICS OF SE LORETO FAULT ARRAY

The objectives of our kinematic analysis are to: (1) determine if the fault array is coherent, and (2) determine the kinematics of the SE Loreto fault array.

Fault array coherence

Due to the geometry, kinematic interdependence and consistency in orientation of faults in the SE Loreto fault array, the entire array is considered geometrically and

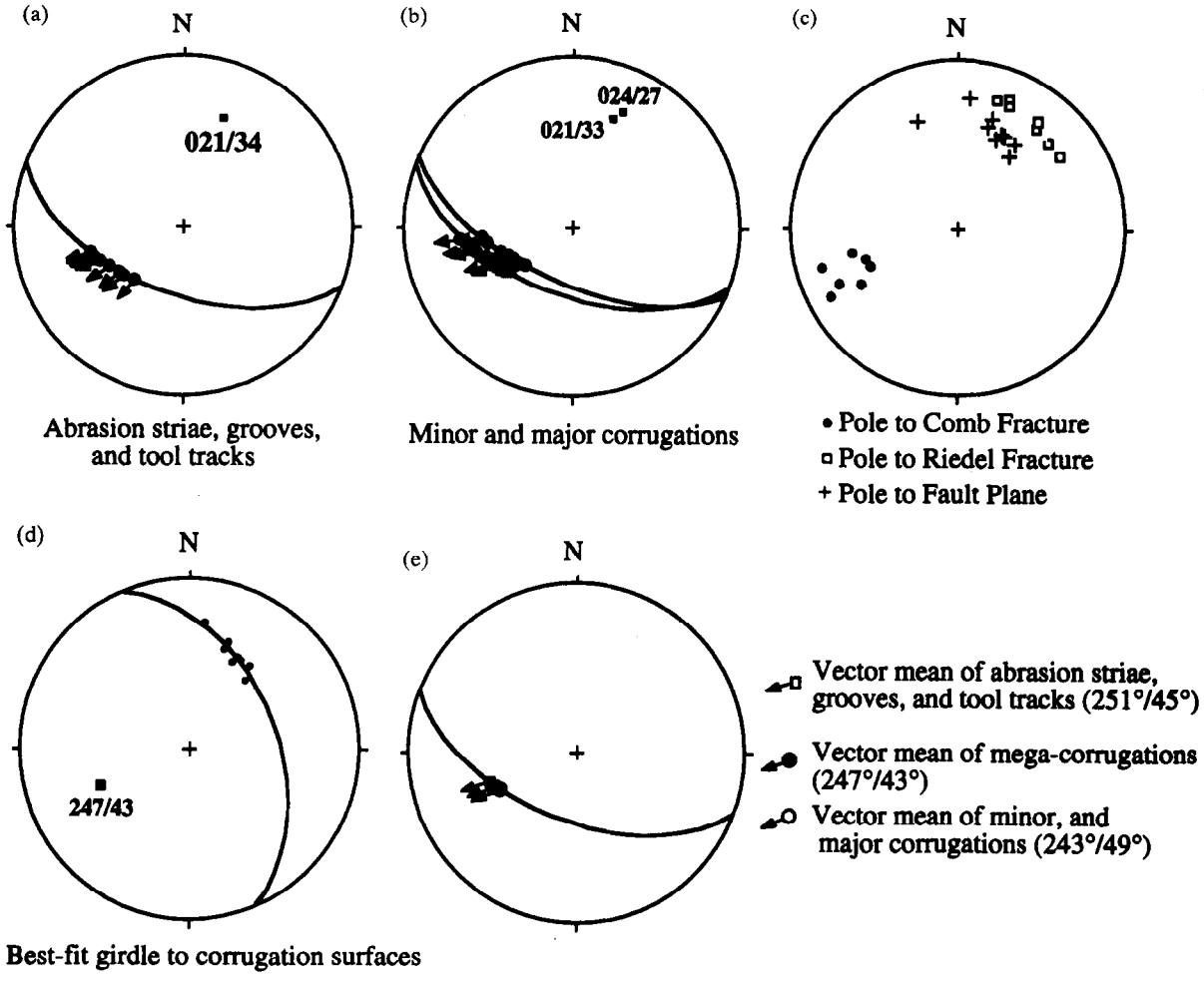

Fig. 7. Summary of kinematic data for the Corrugation fault. (a) Small-scale striae; (b) minor and major corrugations; (c) poles to fractures and fault poles; (d) best-fit girdle to corrugation surfaces; and (e) comparison of vector means for all lineations. Ball and arrow symbol represents the trend and plunge of each lineation and the relative movement of the hangingwall. Note close correspondence of all lineations.

kinematically coherent. Geometric coherence refers to the geometric interdependence of faults, which is evidenced by complimentary variations in offset along fault lengths and splays, and the continuity of dip- and strike-linked fault segments (Walsh & Watterson 1991). The splayed and interconnected nature of faults in the study area is representative of what Walsh & Watterson (1991) called 'hard-linked', that is faults whose surfaces are linked on the scale of the map or cross-section such that mechanical continuity is achieved by the interaction of related fault surfaces rather than strain between faults (Fig. 3). Faults that splay into and/or are on strike with other fault segments are considered 'strike-linked' and if faults splay and merge at depth they are considered 'dip-linked'. Extrapolating fault dips to shallow depths suggests that many faults behave in a 'dip-linked' fashion (Fig. 10). These geometric relationships, coupled with the fact that displacement on faults and related splays is complementary or conservative (that is net displacement is constant along any one fault segment or splay), suggests that the fault array is geometrically coherent.

One importance of geometric coherence lies in the inference that a similar degree of coherence existed during the development of the array. Walsh & Watterson (1991) suggested that the timing and rates of displacement along any one fault or splay is similar to that of all other faults in a geometrically coherent array. The geometric coherence of the SE Loreto fault array suggests that it developed synchronously as one array rather than a series of separate sub-arrays. Local cross-cutting relations and the inferred age of strata support fault array coherence, because they suggest that most of the faulting occurred over only ~400,000 years from ~2.4 to 2.0 Ma (Umhoefer *et al.* 1994a). Local relations allow that domain 1 faulting started before much of the domain 2 faulting in the east, so that initiation of faulting may have migrated from west to east across the fault array.

Method

The fault data used for kinematic analysis consisted of fault plane orientation, sense of separation and the direction of slip. Sense of separation was determined by mapping of stratigraphic relationships and *S–C* composite structures developed in carbonate fault gouge. Abrasion striae and grooves provided the best indicators of the sense of slip. Many workers (e.g. Rutter *et al.*

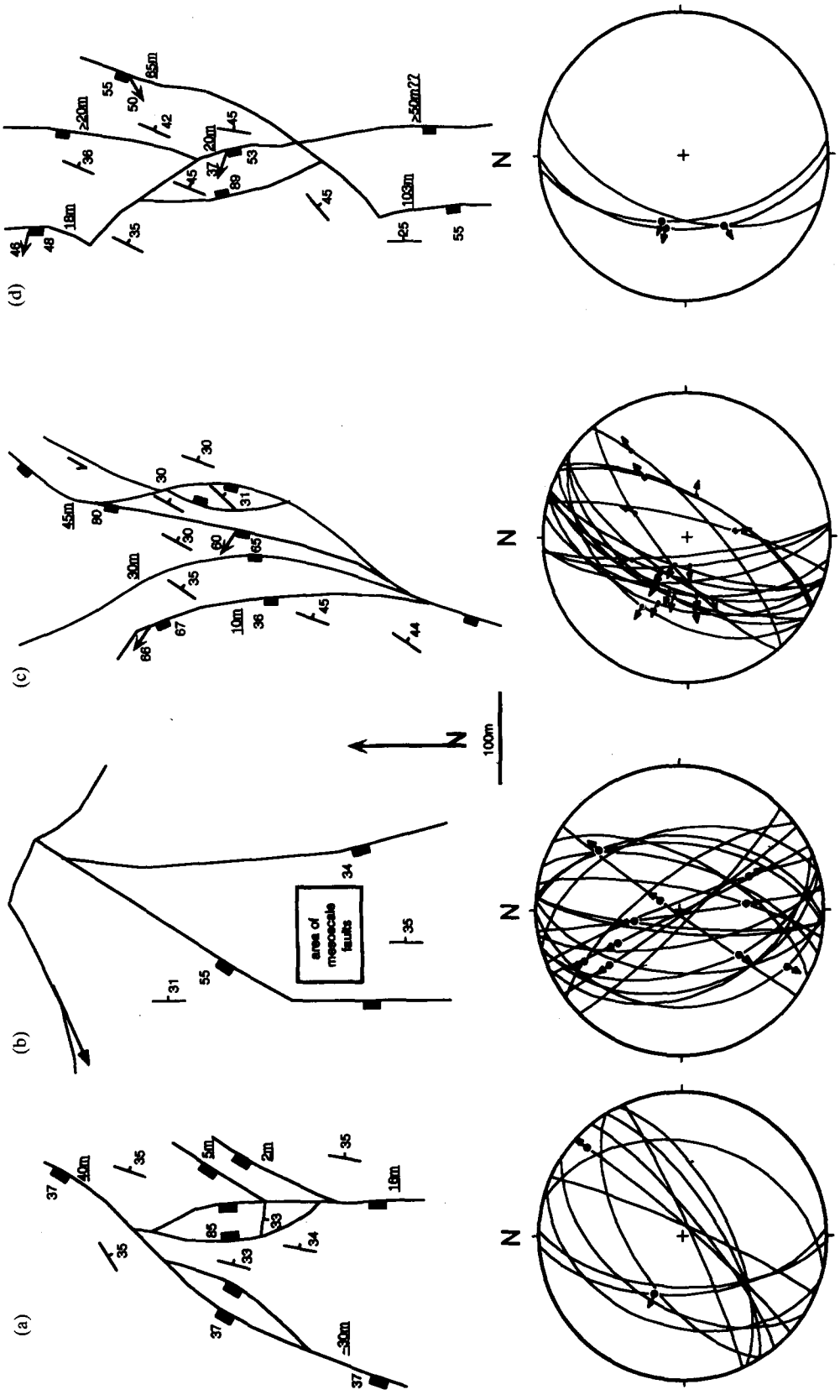

Fig. 8. Maps and kinematic data from four areas within the SE Loreto fault array that are interpreted to be more complex because of strain accommodation. The areas are labeled on Fig. 3. Stereonets correspond to maps above and show fault planes and striae with ball-and-arrow. Arrow indicates movement of upper plate of fault. Arrows on faults are azimuth of fault motion on oblique slip faults as determined from kinematic indicators on the fault. Numbers near arrows are the plunge of the fault lineations. Rectangles are on segments that have subvertical slip. Strike and dips are for bedding.

1986, Chester & Logan 1987, Ramsay & Huber 1987, Marrett & Allmendinger 1990), however, caution against relying too much on striae preserved on faults with thick gouge zones (>50 cm) and hundreds of meters of offset. They argue that striae can be fundamentally ambiguous and/or only record the last movement on the fault, which may not represent the overall finite slip vector. We argue that, because a majority of the faults making up the SE Loreto fault array have relatively thin carbonate gouge and fault breccia zones (5–10 cm, 15–35 cm, respectively) and offsets typically average <50 m, the striae preserved do represent finite slip. This is further supported by several other observations: (1) there is very limited evidence to suggest multi-phase deformation (i.e. multiple sets of striae on fault surfaces); (2) based on age constraints on faulting (Umhoefer *et al.* 1994b), the SE Loreto fault array formed synchronously in one relatively short event, and thus the striae observed on fault surfaces must belong to the same generation; (3) striae on smaller faults with a few tens of centimeters of offset will, by virtue of their size and limited formation time, represent the finite slip vector; the orientations of these striae are consistent with striae preserved on larger-scale faults; and (4) the consistency between different types and sizes of fault lineations, including striae, on the Corrugation fault suggests that striae are a reliable indicator of sense of slip (Fig. 7).

For strain analysis of brittle faults we used the kinematic analysis of fault-slip data of Marrett & Allmendinger (1990). This method determines a direction of maximum shortening and maximum extension for each fault. Each fault is treated as if it contributed an incremental strain to the bulk strain of the fault array or domain analyzed. The strain axes for individual faults are then contoured to give principal strain axes for the array or domain. The strain analysis method of Marrett and Allmendinger is a seismological approach in which the principal strain axes are equivalent to pressure and tension axes of fault-plane solutions.

The strain analysis assumes that: (1) the fault array is scale invariant; (2) the faults were not reoriented after they formed; and (3) the sampling is representative of the whole fault array (Marrett & Allmendinger 1990). Assumption (3) is generally true because of the excellent exposure in the fault array and the high percent of fault segments that yielded kinematic data.

Assumption (1) can be tested by a weighting method (Marrett & Allmendinger 1990). One can test scale invariance qualitatively by analyzing the kinematics of faults of different sizes. The data set from the SE Loreto fault array is barely adequate for this test, but does have data over 2 (+) orders of magnitude. Faults with <1 m offset are locally common in the strain accommodation zones, but data necessary to determine moment tensor summation, such as fault thickness, was deemed unreliable because it varied widely on individual faults. The results of linked Bingham distribution and moment tensor summation of those faults with adequate data from three size groups show close grouping of the extension and shortening axes (Fig. 9 and Table 1). We tentatively conclude that the faults of the array are scale invariant.

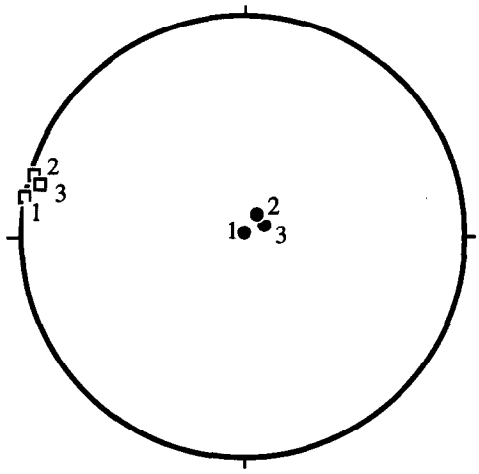

Fig. 9. Shortening axes (filled circles) and extension axes (open squares) for three sizes of faults. This constitutes a weighting test that suggests that the fault array is scale invariant (Marrett & Allmendinger 1990). Each point represents a group of faults as shown in Table 1. See Table 1 for data.

Assumption (2) is generally true in the SE Loreto fault array but may well be violated to a limited extent. The fault array represents one faulting episode as shown by the geometric and kinematic coherence as discussed below. Faulting is restricted to a few 10^5 years in the late Pliocene, from ~2.4 to ~2.0 Ma (Umhoefer *et al.* 1994b). If the faulting developed systematically from west to east as is possible, then older, inactive faults to the west may have been tilted in the hangingwall of younger faults to the east and violated this assumption. However, because all the faults have offsets of 200 m and less (and most are <50 m), and large parts of the array are linked, the faults that may have been tilted in the hangingwall were probably at least hundreds of meters

Table 1. Weighting test by comparing the kinematics of faults of three different sizes using moment tensor summation and linked Bingham distribution statistics. Directions in trend and plunge

Offset (m)	No. of faults	Moment of tensor summation		Linked Bingham maxima	
		Shortening	Extension	Shortening	Extension
100–200	2	010°, 89°	280°, 00°	010°, 89°	280°, 00°
10–100	15	029°, 81°	286°, 02°	029°, 81°	286°, 02°
1–10	12	062°, 82°	284°, 06°	062°, 82°	284°, 06°

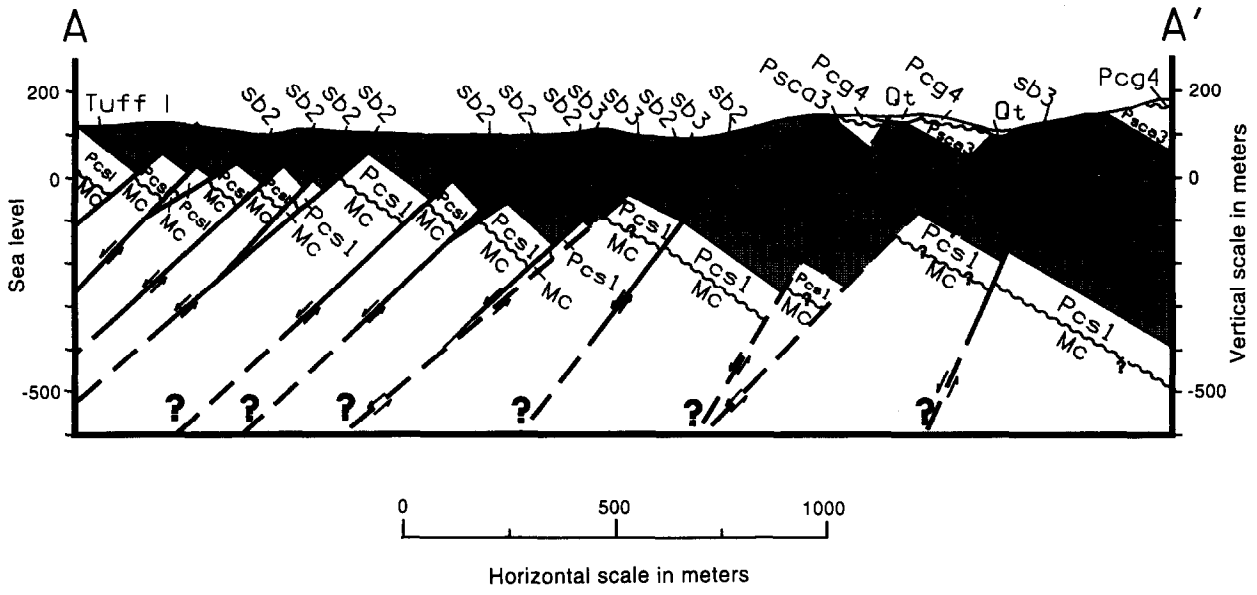

Fig. 10. Cross-section across southern part of domain 2. Map units are the same as in Fig. 3, except Qt, which is Quaternary terrace. Location of section in Fig. 3.

away from active faults and therefore tilted a few degrees at most.

Domains 1 and 2

Faults in domain 1 are characterized by a dextral strike-slip component. Rakes of striae range between 9° and 175° (right-hand rule) for W-dipping faults, and average 110° if all faults are included (Fig. 11). Thus, fault movement ranged from sinistral slip to dextral slip, but only a small number of faults show the former (Figs. 12a & c). The largest faults in this domain are not represented by this mean vector, but separately they have an average rake of about 150°, or dextral-normal slip. Smaller faults have more dip-slip movement. There is also a good correlation between fault strike and sense of obliquity in domain 1 (Figs. 12a, c, d & e). There is less of a correspondence between dip and rake, but a general trend does suggest that the steeper faults have more dextral slip (Figs. 11 and 12b). In sum, in domain 1 the NW-striking faults are longer and have large offset (tens to a few hundreds of meters offset), exhibit dextral-normal to dextral-strike-slip behavior, and are steeply inclined. Northerly striking faults are smaller (meters of offset), more dip-slip and moderately inclined, and the NE-striking faults are also smaller and dominantly sinistral-oblique-slip.

Domain 2 contains faults that exhibit more uniformity in both orientation and direction of fault slip than domain 1. An equal number of faults show both normal-sinistral and normal-dextral slip with a large percentage of faults exhibiting almost pure dip-slip behavior (Figs. 11 and 12f). Rake values for domain 2 range from 25° to 135°, but the majority of rake values are 90° ± 10° (Figs. 12f & g). Although the scatter observed in a rake vs strike of faults plot for domain 2 indicates little statistical significance, general trends similar to those of domain 1 can be seen. Overall, NW-striking faults are dominantly dextral-oblique to dextral strike-slip (Figs. 12e & j), N-striking faults are dip-slip (Figs. 12d & i), and NE-striking faults are sinistral-oblique-slip (Figs. 12c & h). However, unlike in domain 1, the extension direction in domain 2 does not vary with strike (compare Figs. 12h & j). The two WNW-striking transfer faults in domain 2 fit this pattern as they had strongly dextral-normal slip (Fig. 3).

Thus, the data for both domains suggest that the kinematic behavior of faults is dependent on their orientation relative to the direction of extension for the SE Loreto fault array and further supports the kinematic coherence of the fault array. North- to NNE-striking faults are almost all west dipping and nearly pure normal slip. More NE-striking faults show normal-sinistral slip and NW- to WNW-striking faults show dextral-normal slip.

DIRECTION AND AMOUNT OF EXTENSION

Direction of extension

The majority of faults in the SE Loreto fault array strike N to NNE and display normal slip, suggesting an E–W to ESE–WNW bulk extension direction. This qualitative observation has been further substantiated by strain analysis of the kinematic data. Following Marrett & Allmendinger (1990), we determined the extensional strain axes for all fault plane-striae pairs and then combined the data in each domain to determine an extension or tension axis (Fig. 13), similar to the P and T axes of fault-plane solutions in seismology (graphical analyses of fault-slip data used the program Faultkin from Allmendinger, Marrett and Cladouhos). It is argued that because the P and T axes are fundamentally kinematic in nature, they can be used to represent the

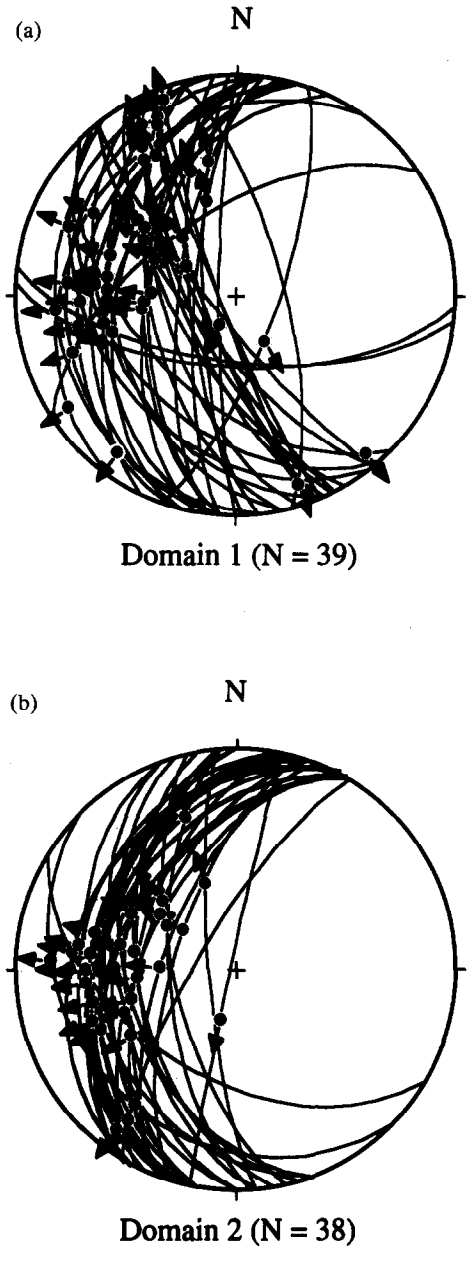

Fig. 11. Equal-area lower-hemisphere stereograms of faults and striae for domains 1 and 2. Great circle represents fault plane, ball and arrow represents trend and plunge of striae and relative movement of the hangingwall.

axes of incremental strain (Marrett & Allmendinger 1990).

Domain 1 composite fault-plane solution shows a small component of dextral oblique-slip behavior, but dominantly dip-slip motion, with a *P*-axis orientation (i.e. trend and plunge) of 016°/71°, and a *T*-axis orientation of 281°/2° (Fig. 13a). The domain 2 fault-plane solution shows essentially dip-slip behavior, with a *P*-axis orientation of 164°/87° and a *T*-axis orientation of 274°/1° (Fig. 13b). A cumulative plot of all kinematic data for the SE Loreto fault array gives a fault plane solution with a slight dextral-oblique component, and *P* and *T* axes orientations of 027°/85° and 278°/2°, respectively (Fig. 13c). Thus the bulk extensional strain is E–W to slightly ESE–WNW. A cumulative contour diagram for both *P* and *T* axes for domains 1 and 2 shows a uniform distribution of data (i.e. maxima are not multimodal) (Fig. 14), which further supports the notion of kinematic coherence and spatial homogeneity for the SE Loreto fault array (after Marrett & Allmendinger 1990). Moreover, the similarity in *T*-axis orientation for domains 1 and 2 also supports the assertion of kinematic coherence. We do note, however, that domain 1 has a more northwesterly extension direction and may be the oldest faulting in the array (Umhoefer *et al.* 1994b). Thus, the extensional direction may have rotated a small amount counterclockwise during development of the fault array.

The overall extension direction of 278–98° is similar within a few degrees to the σ_3 direction derived from paleostress analysis in two areas only 1–2 km west of the SE fault array (Zanchi 1994). It is also similar to the E–W direction of σ_3 that Angelier *et al.* (1981) obtained from paleostress analysis of faults cutting Pliocene strata of the Santa Rosalia basin ~200 km north of the Loreto basin.

Amount of extension

The amount of horizontal extension for the SE Loreto fault array was determined using two methods: (1) simple line balancing of key marker beds or piercing points; and (2) the geometrical method of Axen (1988). Because of the significant dextral strike-slip component in domain 1, cross-sections for determination of extension were only used across domain 2. Therefore the component of extension contributed by the strike-slip faulting is not accounted for here. We present results from the most well constrained cross-section across the southern part of the study area (Fig. 10; location on Fig. 3).

Several key marker horizon lengths, especially unique shell beds, in the cross-section were measured (Fig. 10). Their total length was assumed to be equal to L_0, the original length before extension. This cumulative line-length was then compared to that of L, the line-length representative of the extended distance between undeformed terrain and that of the last known fault affecting the area. The simple ratio $(L - L_0/L_0) \times 100$ was then used to calculate the percent horizontal extension (%HE). By this method the horizontal extension is 32%. Accuracy of the line-balance method depends on how well-constrained the cross-section data are for the analysis. For this study, detailed surface mapping provided very good control on bedding and fault orientation, bedding thickness and fault offset. Although few assumptions went into cross-section construction, certain assumptions had to be made about bedding thickness at depth (constant bedding thickness was assumed at these shallow depths), and offset on faults that were poorly exposed in the field (although these accounted for less then 10% of the faults in the cross-section). Because the cross-section is well-constrained, neither of the above assumptions will propagate significant error.

The geometrical method (Axen 1988) considers non-parallel, unevenly spaced domino-style faults situated

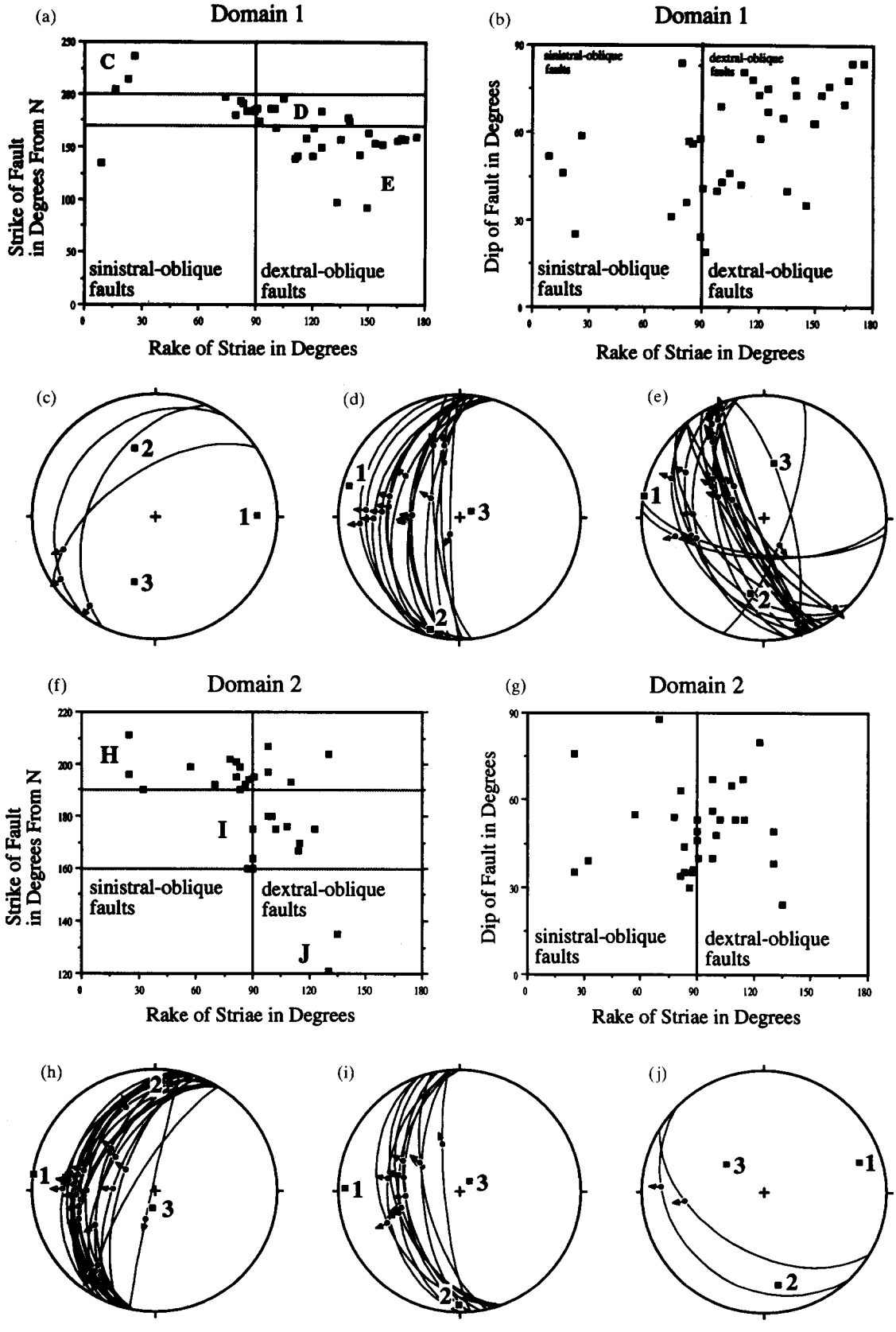

Fig. 12. (a) Strike vs rake of W-dipping faults of domain 1. Rake values have been plotted using right-hand rule convention. Note that these W-dipping faults are 99% of those in the fault array. (b) Dip vs rake of W-dipping faults of domain 1; (c–e) are stereonets of fault plane and striae sets from domain 1 grouped by strike. The groups and boundaries are labeled with the appropriate stereonet letter within graph (a). Note the systematic change in the arrangement of linked Bingham axes (1, 2, 3), which change from sinistral-extension (c) to pure extension (d) to dextral-extension (e) with changing strike. (f) Strike vs rake of W-dipping faults of domain 2. (g) Dip vs rake of W-dipping faults of domain 2; (h–j) are stereonets of fault plane and striae sets from domain 2 grouped by strike. The groups and boundaries are labeled with the appropriate stereonet letter within graph (f). Note that the linked Bingham axes change little with strike in this domain.

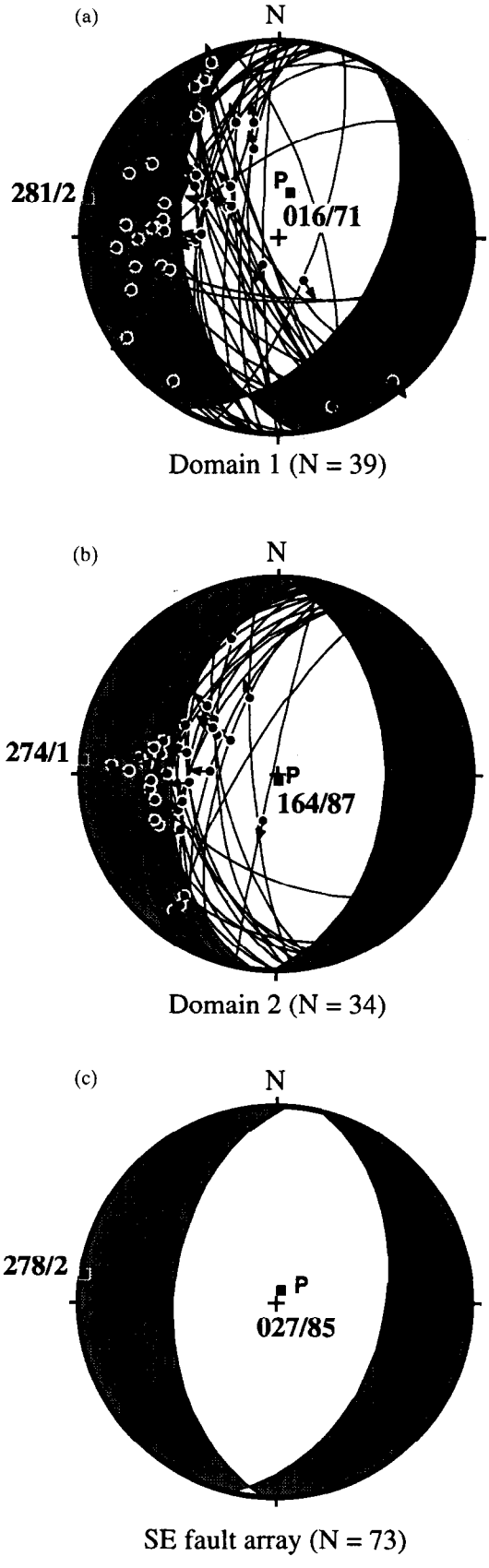

Fig. 13. Equal-area stereograms of faults and striae for domains 1 (a) and 2 (b) superposed onto a fault plane solution of the same data for comparison of the extension (T) and compression (P) axes orientations. Great circles represent fault planes; ball and arrow symbol represents trend and plunge of striae and the relative movement of the hangingwall. Numbers (e.g. 281/2) represent the trend and plunge of each respective P or T axis. (c) The cumulative plot shows only the fault plane solution and has a T axis of 278°/2° and P axis of 27°/85°.

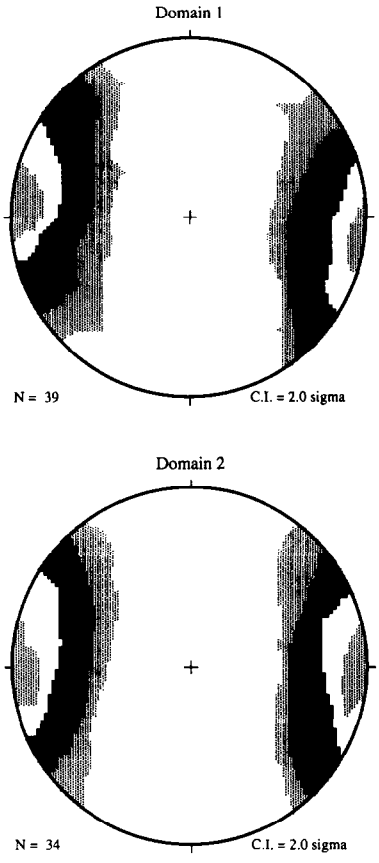

Fig. 14. Stereonets of contours of T (extension) axes from domains 1 and 2. Note that they form a simple cluster.

above a dipping or flat basal detachment. The model depends on five primary assumptions: (1) the existence of a fault-normal detachment at depth, either horizontal or dipping; (2) domino-style normal faults and the basal detachment are planar; (3) fault blocks are rigid and do not deform internally; (4) no large translations have occurred on the detachment subsequent to domino-style faulting; and (5) all faults moved simultaneously. For the SE Loreto fault array, assumptions (3) and (5) are considered valid as discussed previously. Because there is little or no control on the fault geometry at depth and the orientation of the Loreto fault is also uncertain, assumptions (1) and (2) are untested; mapping suggests that the SE Loreto fault array continues to the south and may eventually merge with the Loreto fault, thus requiring them to have an antithetic–synthetic relationship. Assumption (2) may be partially violated if the faults are slightly listric. A small listric component is suggested because (i) some of the faults curve gently in map view, and (ii) the relationship between the dip of beds and percent extension from line balancing suggests a small listric component (after Wernicke & Burchfiel 1981). For the purpose of these calculations, however, the faults are assumed to have a planar geometry and merge into a horizontal detachment at depth. Finally, assumption (4) is considered valid because there is no compelling reason to believe that any large-scale faulting on the Loreto fault occurred after faulting in the SE array.

Unlike parallel domino-style faults, non-parallel and unevenly spaced domino-style faults have a different amount of extension across each fault block. Thus, Axen (1988) used a simple weighted summation derived from Thompson's (1960) equation, which relates the amount of rotation of beds (θ), the final fault dip (ϕ) and e_m (the ratio of the horizontal distance between similar piercing points a_m, and total extension length L, that is, $e_m = a_m/L$):

$$\%\mathrm{HE} = \sum_{m=1}^{n} [\sin(\phi_m + \theta)/\sin\phi_m - 1](e_m) \times 100.$$

For the cross-section, a weighted summation was calculated, assuming non-parallel fault geometry and a horizontal fault-normal detachment at depth.

The amount of horizontal detachment from the geometric technique for the cross-section is 39%, as compared to the result from line-balancing of 32% extension. This discrepancy probably results from the breakdown of assumption (2) of the geometrical method as outlined above. Thus, it is concluded that the best estimate of a minimum percent-extension across the SE Loreto fault array is from the line-balance method, or 32%.

Our estimate of 32–39% extension across the south-central part of the SE fault array (Fig. 10) compares to an estimate of 45% extension across part of the fault array by Zanchi (1994). Our section A–A′ is nearly in the same position as Zanchi's section C–C′, but extends ~500 m farther west and ~300 m farther east. The primary difference between the two estimates of extension is due to the oblique-slip fault that Zanchi's section D–D′ crosses (east part of his composite section). Our crude estimate of extension on Zanchi's section C–C′ is ~33%, which is close to our best estimate of 32% and overlaps the range of our two estimates using different methods. Because of the complex facies relations and buttress unconformity where our sequence 3 is exposed across the northern part of the fault array (Fig. 3), and the uncertainty of estimating the amount of slip on oblique faults, we caution against quantifying extension across the northern part of the fault array. Zanchi's attempt to estimate extension across the oblique-slip fault emphasizes the fact that our section A–A′ does not cross any oblique-slip faults and therefore we cannot estimate the contribution of those faults.

SE LORETO FAULT ARRAY AS TEST OF OBLIQUE-RIFT MODELS

The study of the SE Loreto fault array provides a well-constrained test of recent oblique-rift models, but only if it is representative of strain along the margin of the Gulf of California. Here we reiterate the arguments given above for this relatively small fault array (~18 km^2) being representative of regional strain: it is well exposed and therefore our detailed mapping defined the fault array in a comprehensive way; the array is geometrically and kinematically coherent and therefore probably developed in a simple manner; the overall extension direction from our study is similar within a few degrees to the extension direction derived from paleostress analysis from previous, but less detailed, studies of the Loreto basin (Zanchi 1994) and Santa Rosalia basin (Angelier *et al.* 1981); the SE fault array is interpreted to be a transfer zone between the southern Loreto fault and a coastal fault to the north and therefore it is part of a much larger fault system.

The SE fault array, if representative of regional strain, is a direct consequence of interaction between the North American and Pacific plates and therefore may record that relative plate motion if the fault patterns from modeling are correct. Specifically, oblique rifting of the Gulf of California has produced a series of faults and basins within the Gulf Extensional Province in the Pliocene to Quaternary (Fig. 1), one of which is the Loreto basin and SE Loreto fault array of this study. Analytical and physical models of oblique extension have been used to predict fault trends and the direction of extension for differing amounts of obliquity in rift settings (Withjack & Jamison 1986, Tron & Brun 1991, Smith & Durney 1992). Here we compare the SE Loreto fault array to this modeling.

The analytical modeling (McCoss 1986, Withjack & Jamison 1986, Tikoff & Teyssier 1994) suggests that there is a significant change along oblique-rifted margins from strike-slip-dominated deformation to pure-shear-dominated deformation (mixed strike-slip and normal-slip) where the angle between the rift trend and divergence or plate motion direction (α) equals 20°. These models assume homogeneous strain and constant volume at small strains. This change at 20° is the critical angle of displacement of Smith & Durney (1992). In Withjack & Jamison's (1986) analysis, the critical angle varies with the Poisson's ratio. In these models, the horizontal principal strain is the greatest extensional strain for all values of α in the models. Corresponding to the change from strike-slip-dominated deformation to pure-shear-dominated deformation at $\alpha = 20°$, the second horizontal principal strain axis is the greatest contractional strain for $\alpha < 20°$, whereas for $\alpha > 20°$ the vertical strain is the greatest contractional strain (Withjack & Jamison 1986, Tikoff & Teyssier 1994).

The critical angle varies considerably in experimental data from 30° (Withjack & Jamison 1986) to 45° (Smith & Durney 1992) to a range from 30° to 60° (Tron & Brun 1991). This variation is probably due to the differences in the experimental apparatus in each experiment, particularly different boundary conditions (Smith & Durney 1992). The experiments also varied in the size of the intervals between α in successive experiments (Smith & Durney 1992). Smith & Durney (1992) analyzed the critical angle using a model that takes into account the dilatancy that occurs at initiation of faulting. Their model predicts the critical angle when there is no vertical strain because of the dilatancy.

To calculate α for the Loreto basin, we measured a rift trend of 325° for the southern Gulf of California

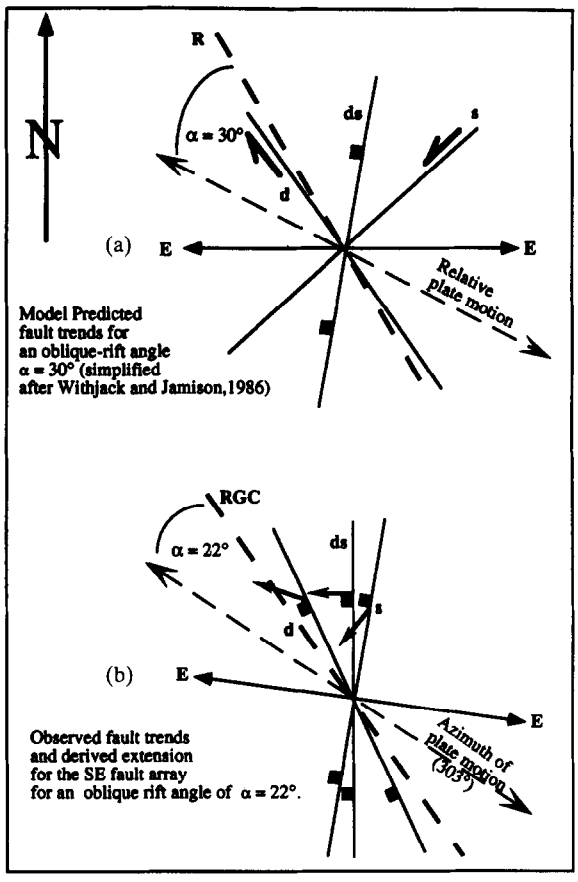

Fig. 15. Comparison of experiment-derived (Withjack & Jamison 1986) fault patterns for $\alpha = 30°$ to that of observed fault patterns for the SE fault array ($\alpha = 22°$). R: modeled rift trend; RGC: rift trend of the Gulf of California (325°); E: extension direction; s: sinistral-normal-slip fault; d: dextral-normal-slip fault; ds: dip-slip fault.

transform-rift system. The Pacific–North America plate motion in the southern Gulf of California is 303° as determined by GPS (Dixon *et al.* 1991), 306° by the NUVEL I global plate-motion model (DeMets *et al.* 1990), 307° by VLBI (Argus & Gordon 1991) and 310° by a plate-motion model for the past 5.5 Ma (Stock & Hodges 1989). Therefore, α for the Loreto basin region is between 15° and 22°, depending on the value used for plate motion, or close to the theoretical critical angle of displacement.

The geometry of faults in the SE Loreto fault array most closely resembles Withjack & Jamison's (1986) experiment when $\alpha = 30°$ (Fig. 15), the first experiment they did above the $\alpha = 20°$ critical angle. In the $\alpha = 30°$ experiment, ~10% of faults were combined synthetic strike-slip–normal-slip and strike subparallel to the rift trend (dextral-normal with a strike of 325° in a dextral-oblique plate margin such as near Loreto), ~10% of faults are antithetic strike-slip–normal-slip and strike 50–60° from the rift direction (away from plate-motion direction or clockwise for Loreto or sinistral-normal with a strike of 015–025°), and ~50% of faults are dominantly normal slip and strike 005–050° away from the rift trend (normal with a strike of 330–015° for Loreto). These experimental results are remarkably similar to the SE Loreto fault array (Fig. 15), where a small number of faults in domain 1 are dextral-normal slip and strike 320–335°, most of the faults in the array are normal slip with strikes from 315 to 040°, but averaging ~010°, and the more northeasterly striking faults are sinistral-normal slip (Figs. 11 and 12).

At face value, the results from the SE Loreto fault array seem to differ only a little from analytical results when the α angle is considered. The fault orientations and kinematics in the SE Loreto fault array are most similar to the experiment at $\alpha = 30°$, while the calculated α for the Loreto region was 15–22°; the α derived from the plate motion from GPS (22°) is closest to the similar modeling result. These differences disappear if we consider recent insights from strain modeling of oblique margins. Tikoff & Teyssier (1994) point out that experimental results are detecting fault patterns that reflect instantaneous strain and when finite strain is considered the nature of the predicted fault array becomes more complex. In strike-slip-dominated deformation near the critical $\alpha = 20°$, strike-slip faults form first in response to instantaneous strain (Tikoff & Teyssier 1994). Continued deformation results in normal faults forming to accommodate the pure-shear component of finite strain. The predictions from combined instantaneous and finite strain suggest that the $\alpha = 15°$ experiments of Withjack & Jamison (1986) would change with continued deformation to approximate the geometric and kinematic data from the SE Loreto fault array. In addition, preliminary information from the fault array suggests that domain 1 faulting, which is dominated by dextral-oblique faults, may have been active before faulting in domain 2. This evolution from strike-slip to normal faulting in the SE Loreto fault array matches the evolution of structures predicted from strain modeling (Tikoff & Teyssier 1994).

The direction of bulk extension from Loreto is also similar to the modeling (Withjack & Jamison 1986). The α values of 22–15° for Loreto result in a predicted direction of greatest horizontal extension of 269–272.5° (the extension direction is about halfway between the plate motion and the normal to the rift trend, Withjack & Jamison 1986). The extension in the SE Loreto fault array was 273° for domain 2, the majority of the faults, 281° for domain 1, and 278° for the whole array. Thus, SE Loreto extension was in a direction equal to or up to ~10° clockwise, or toward the rift trend, from that predicted. However, in the modeling of Withjack & Jamison (1986), the ideal extension direction, used above, is for a relative plate displacement that is much less than the width of the original rift zone. The extension direction becomes systematically closer to the rift trend by up to ~10° when the amount of displacement of the plate margin increases and approaches the width of the original rift zone. The displacement to rift-zone-width ratio is not well known for the Late Pliocene when the SE Loreto faulting occurred, but any significant displacement of the plate margin would make the predicted extension direction even closer to the actual extension in the SE Loreto fault array.

The model results of Withjack & Jamison (1986) more closely resemble the SE Loreto fault array than the

experimental results of Tron & Brun (1991) or Smith & Durney (1992). Withjack & Jamison's (1986) experiments employed uniform stretching of a rubber sheet at the base of a clay layer. Smith & Durney's experiments used clay over boards made of Perspex. Tron & Brun (1991) used displacement along a narrow zone below a silicone layer, which lay below an upper layer of sand; movement was transferred by viscous coupling at the base of the sand. In both the geometry and kinematics of structures, the Loreto basin results support a model of homogeneous deformation (similar to the uniform-stretching Withjack & Jamison 1986 model) in the early phase of the modern Gulf of California. Homogeneous deformation may be explained because the tensile strength of rocks is much lower than the compressive strength (Jaeger & Cook 1976), and therefore strain partitioning is less likely in transtensional plate margins such as the Gulf of California. Why the Loreto results resemble the Withjack & Jamison (1986) rather then the Smith & Durney (1992) experiments, both of which used clay is unclear to us. Perhaps it was the differences in boundary constraints employed (Smith & Durney 1992).

Low or no strain partitioning is also supported by a comparison of our results to the analysis of oblique plate motion and strain partitioning by Teyssier *et al.* (1995). If the extension in the SE Loreto fault array represents instantaneous strain, then the rift trend of 325° and the extension of 273° for most of the array (domain 2) or 278° for the entire array results in a maximum instantaneous strain (θT) of 52–47°. Given that α = 15–22° and θT = 52–47°, virtually no partitioning is predicted (fig. 3 of Teyssier *et al.* 1995).

DISCUSSION

From our field study of the SE Loreto fault array and comparison to modeling results, we infer that the early part of the modern stage of southern Gulf of California transform-rifting (pre-~2 Ma), when most of the SE Loreto fault array formed, included only minor regional strain partitioning and was a largely homogeneous system. Homogeneous deformation suggests that any large strike-slip faults had low slip rates. The extension in the SE Loreto fault array was similar to the extension direction predicted from simple modeling of homogeneous oblique rifting after significant displacement. This conclusion of low rates of strike-slip faulting before ~2 Ma is contradicted by some estimates of large-scale faulting in the Gulf since before 5 Ma (e.g. Humphreys & Weldon 1991, Powell & Weldon 1992).

Perhaps pre-2 Ma strike-slip faulting was on many smaller faults across the wide rift zone. As the plate margin evolves, the rift segments and transform faults formed in their modern configuration and the margin very quickly evolved to complete strain partitioning, with all of the strike-slip component of the plate motion occurring along the transform faults. This change occurred at ~2.5–2.0 Ma in the southern Gulf of California (Lonsdale 1989), about the same time as most of the faulting in the SE Loreto fault array. The extension direction within the plate margins during this final stage with near-complete partitioning should swing toward a direction nearly perpendicular to the rift trend (WSW or ~240–245° along southern Gulf of California) (Teyssier *et al.* 1995). Indeed, we have found a late Quaternary fault scarp that strikes ~350°. If the fault scarp has pure normal slip, then it has an extension direction of ~260°. This extension direction does not precisely fit the previous hypothesis, but it does hint at a rotation of extension direction from the late Pliocene to late Quaternary time, due to the formation of the transform faults in the deep Gulf of California.

Positive field tests of analytical and experimental models of oblique rifting, such as ours, make the predictive power of the models much greater. If the relation between strain patterns and kinematics in brittle fault arrays and plate motion can be constrained better along young plate margins, then the geometry and kinematics of structures in ancient mountain belts, where plate motion is unknown, may be used to determine the approximate obliquity of ancient plate motions.

CONCLUSION

(1) Due to the strike-linked and presumably dip-linked nature of the SE Loreto fault array, mechanical continuity between faults was achieved by the interaction of related fault surfaces rather than distributed strain between faults, and thus the array is considered geometrically coherent. This in turn would imply that a high degree of kinematic coherency or synchronous fault movement occurred during the evolution of the array. The kinematic analysis supports this coherence.

(2) Kinematic behavior of faults is a simple function of their orientation relative to the direction of bulk extensional strain. Uncommon NE-striking faults are dominantly sinistral-normal, common north-striking faults are dip-slip, and locally common NW-striking faults are dextral-normal to dextral strike-slip.

(3) Direction of bulk extensional strain as determined by converting kinematic data into a fault-plane solution yields an extension azimuth of 281–101° for domain 1, 274–094° for domain 2 and 278–098° for the entire SE Loreto fault array.

(4) The amount of extension as determined by a simple line-balance method of key piercing-points across the southern part of the study area yields 32%.

(5) Despite the small size (~18 km^2) of the SE Loreto fault array, the geometric and kinematic coherence, simple and consistent kinematic behavior, short duration of activity, link to major fault zones to the north and south, and similarity of the SE fault array extension direction to other results in the region, all suggest that the faulting was representative of the regional strain pattern in the uppermost crust along the Gulf of California during late Pliocene time.

(6) If conclusion (5) above is correct, then it is relevant to compare our results to those from modeling of

oblique rifting. The angle of obliquity of rifting determined for the southern Gulf of California (α = 22–15°) and the geometric and kinematic nature of the SE Loreto fault array is in good agreement with physical and analytical models of oblique extension, especially those of Withjack & Jamison (1986), when we also consider the insights from strain modeling of oblique plate margins (Tikoff & Teyssier 1994).

(7) This positive field test of the first-order results of modeling suggests that kinematic analysis and fault patterns of brittle fault arrays have the potential to provide estimates of the obliquity of rifting in ancient orogens where the azimuth of plate motion is unknown.

Acknowledgements—Supported by National Science Foundation grants EAR-9296255 (P. J. Umhoefer) and EAR-9117269 (Rebecca Dorsey) and the Northern Arizona University Friday Lunch Clubbe (K. A. Stone). We thank Kathy Carder for drafting help, Joann Stock, Claudia Lewis, Gary Axen and Hugh McLean for useful discussions, Ernie Duebendorfer for a helpful early review, and Joann Stock, Andrea Zanchi and Associate Editor Jim Evans for thorough reviews of the final manuscript. We particularly thank Becky Dorsey for her vital assistance during all phases of our Loreto basin research. P. J. Umhoefer thanks Christian Teyssier and Basil Tikoff for stimulating exchanges about strain modeling.

REFERENCES

Anderson, E. M. 1951. *The Dynamics of Faulting and Dyke Formation with Applications to Britain*, 2nd edn. Oliver and Boyd, Edinburgh.

Angelier, J., Colletta, B., Chorowicz, J,. Ortlieb, L. & Rangin, C. 1981. Fault tectonics of the Baja California Peninsula and the opening of the Sea of Cortez, Mexico. *J. Struct. Geol.* **3**, 347–357.

Argus, D. F. & Gordon, R. G. 1991. Current Sierra Nevada-North America motion from very long baseline interferometry: Implications for the kinematics of the western United States. *Geology* **19**, 1085–1088.

Axen, G. J. 1988. The geometry of planar domino-style normal faults above a dipping basal detachment. *J. Struct. Geol.* **10**, 405–411.

Chester, F. M. & Logan, J. M. 1987. Composite planar fabric of gouge from the Punchbowl Fault, California. *J. Struct. Geol.* **9**, 621–634.

DeMets, C., Gordon, R. G., Argus, D. F. & Stein, S. 1990. Current plate motions. *Geophys. J. Int.* **101**, 425–478.

Dixon, T. H., Gonzalez, G., Lichten, S. M., Tralli, D. M., Ness, G. E. & Dauphin, J. P. 1991. Preliminary determination of Pacific-North America relative motion in the southern Gulf of California using the Global Positioning System. *Geophys. Res. Lett.* **18**, 861–864.

Evans, J. P. 1988. Deformation mechanisms in granitic rocks at shallow crustal levels. *J. Struct. Geol.* **10**, 437–443.

Fitch, T. 1972. Plate convergence, transcurrent faults, and internal deformation adjacent to southeast Asia and the western Pacific. *J. geophys. Res.* **77**, 4432–4460.

Gastil, T. G., Phillips, R. P. & Allison, E. C. 1975. Reconnaisance geology of the state of Baja California. *Mem. geol. Soc. Am.* **140**.

Hancock, P. L. 1985. Brittle microtectonics: principles and practice. *J. Struct. Geol.* **7**, 437–457.

Hancock, P. L. & Barka, A. A. 1987. Kinematic indicators on active normal faults in western Turkey. *J. Struct. Geol.* **9**, 573–584.

Hausback, B. P. 1984. Cenozoic volcanic and tectonic evolution of Baja California, Mexico. In: *Geology of the Baja California Peninsula* (edited by Frizzell, V. A.). *Pacific Section, Soc. Econ. Paleon. Mineral.*, 219–236.

Henry, C. D. 1989. Late Cenozoic Basin and Range structure in western Mexico adjacent to the Gulf of California. *Bull. geol. Soc. Am.* **101**, 1147–1156.

Humphreys, E. D. & Weldon, R. J., II. 1991. Kinematic constraints on the rifting of Baja California. In: *The Gulf and Peninsula Province of the Californias* (edited by Dauphin, J. P. & Simoneit, B. R. T.). *Mem. Am. Ass. Petrol. Geol.* **47**, 217–229.

Jackson, J. 1992. Partitioning of strike-slip and convergent motion between Eurasia and Arabia in eastern Turkey and the Caucasus. *J. geophys. Res.* **97**, 12,471–12,479.

Jaeger, J. C. & Cook, N. G. W. 1976. *Fundamentals of Rock Mechanics*, 2nd edn. Chapman and Hall, London.

Karig, D. E. & Jensky, W. 1972. The proto-Gulf of California. *Earth Planet. Sci. Lett*, **17**, 169–174.

Larson, R. L., Menard, H. W. & Smith, S. M. 1968. Gulf of California: a result of ocean-floor spreading and transform faulting. *Science* **161**, 781–783.

Lister, G. S. & Snoke, A. W. 1984. *S–C* mylonites. *J. Struct. Geol.* **6**, 617–638.

Lonsdale, P. 1989. Geology and tectonic history of the Gulf of California. In: *The Eastern Pacific Ocean and Hawaii: Boulder, Colorado, The Geology of North America* (edited by Winterer, E. L., Hussong, D. M. & Decker, R. W.). *Geol. Soc. Am.* **N**, 499–521.

Lyle, M. & Ness, G. E. 1991. The opening of the Gulf of California. In: *The Gulf and Peninsula Province of the Californias* (edited by Dauphin, J. P. & Simoneit, B. R. T). *Mem. Am. Ass. Petrol. Geol.* **47**, 403–423.

Marrett, R. & Allmendinger, R. W. 1990. Kinematic analysis of fault-slip data. *J. Struct. Geol.* **12**, 973–986.

McCoss, A. M. 1986. Simple constructions for deformation transpression/transtension zones. *J. Struct. Geol.* **8**, 715–718.

McLean, H. 1988. Reconnaissance geologic map of the Loreto and part of the San javier quadrangles, Baja California Sur, Mexico. U.S. Geol. Surv. Map MF-2000, 1:50,000 scale.

Mount, V. S. & Suppe, J. 1987. State of stress near the San Andreas fault: Implications for wrench tectonics. *Geology* **15**, 1143–1146.

Powell, R. E. & Weldon, R. J., II. 1992. Evolution of the San Andreas fault. *A. Rev. Earth Planet. Sci.* **20**, 431–468.

Ramsay, J. G. & Huber, M. I. 1987. *Techniques of Modern Structural Geology, Volume 2: Folds and Fractures*. Academic Press, London.

Rutter, E. H., Maddock, R. H., Hall, S. H. & White, S. H. 1986. Comparative microstructures of natural and experimentally produced clay-bearing fault gouges. *Pure & Appl. Geophys.* **124**, 3–30.

Smith, J. V. & Durney, D. W. 1992. Experimental formation of brittle structural assemblages in oblique divergence. *Tectonophysics* **216**, 235–253.

Spencer, J. E. & Normark, W. R. 1979. Tosco-Abreojos fault zone: A Neogene transform plate boundary within the Pacific margin of Baja California, Mexico. *Geology* **7**, 554–557.

Stock, J. M. & Hodges, K. V. 1989. Pre-Pliocene extension around the Gulf of California and the transfer of Baja California to the Pacific plate. *Tectonophysics* **8**, 99–115.

Teyssier, C., Tikoff, B. & Markley, M. 1995. Oblique plate motion and continental tectonics. *Geology* **23**, 447–450.

Thompson, G. A. 1960. Problem of late Cenozoic structure of the Basin and Ranges. In: *Proceedings of the 21st International Geological Congress*. Det Berlingski Bogtrykkeri, Copenhagen, **18**, 62–68.

Tikoff, B. & Teyssier, C. 1994. Strain modeling of displacement-field partitioning in transpressional orogens. *J. Struct. Geol.* **16**, 1575–1588.

Tron, V. & Brun, J.-P. 1991. Experiments on oblique rifting in brittle–ductile systems. *Tectonophysics* **188**, 71–84.

Umhoefer, P. J., Dorsey, R. J. & Renne, P. 1994a. Tectonics of the Pliocene Loreto basin, Baja California Sur, Mexico, and evolution of the Gulf of California. *Geology* **22**, 649–652.

Umhoefer, P. J., Dorsey, R. J. & Stone, K. A. 1994b. Timing of transtensional deformation in the southern Loreto Basin, Baja California Sur. *Geol. Soc. Am. Abs w. Prog.* **26**, 100.

Walsh, J. J. & Watterson, J. 1991. Geometric and kinematic coherence and scale effects in normal fault systems. In: *The Geometry of Normal Faults* (edited by Roberts, A. M., Yielding, G. & Freedman, B.). *Spec. Publs. geol. Soc. Lond.* **56**, 193–203.

Wernicke, B. & Burchfiel, B. C. 1981. Modes of extensional tectonics. *J. Struct. Geol.* **4**, 104–115.

Withjack, M. O., Islam, Q. T. & La Pointe, P. R. 1995. Normal faults and their hanging-wall deformation: an experimental study. *Bull. Am. Ass. Petrol. Geol.* **79**, 1–18.

Withjack, M. O. & Jamison, W. R. 1986. Deformation produced by oblique rifting. *Tectonophysics* **126**, 99–124.

Wu, D. & Bruhn, R. L. 1994. Geometry and kinematics of active normal faults, South Oquirrh Mountains, Utah: implications for fault growth. *J. Struct. Geol.* **16**, 1061–1075.

Zanchi, A. 1994. The opening of the Gulf of California near Loreto, Baja California, Mexico: from basin and range extension to transtensional tectonics. *J. Struct. Geol.* **16**, 1619–1639.